Nuclear Instruments and Methods in Physics Research A 336 (1993) 510–520
North-Holland

NUCLEAR INSTRUMENTS & METHODS IN PHYSICS RESEARCH
Section A

Characteristics and performance of an electromagnetic shower sampling calorimeter with wavelength shifting fibre readout

D. Autiero, F. Bosi, P. Camarri, V. Cavasinni, T. DelPrete, E. Iacopini and D. Rizzi
INFN, Sezione di Pisa and Dipartimento di Fisica dell'Universita' di Pisa, Pisa, Italy

Received 2 April 1993 and in revised form 2 July 1993

We have studied the properties of electromagnetic shower counters made of scintillator and lead tiles of different thickness. Light collection is achieved by wavelength shifting fibres sparse in the body of the calorimeter. The counters were tested in a beam of electrons, pions and muons with energies between 2 and 8 GeV. We report here the final results of the test. The energy resolution is in good agreement with what is expected from the sampling fraction, i.e. $\sigma/E = 0.07/\sqrt{E}$, the non uniformity of the response is less than 1% at the centre of a counter and 7% in the boundaries between modules, and the π/e contamination is at the level of a few 10^{-3}. Performance of the calorimeter with readout systems able to operate in magnetic field is also reported.

1. Introduction

The electromagnetic shower sampling counters are currently being used for measuring the energy of electrons and photons above a few hundred MeV [1,2]. A counter is made of alternate layers of showering medium and active sampling device. It is however relatively difficult to implement intensive segmentation for position information, without complex light collection systems which inevitably introduce dead space between nearby modules. In our case the light from the scintillator is collected by wavelength shifting (WLS) optical fibres of small diameter which pass longitudinally through the calorimeter [3]. Using this system, the light from a scintillating plate reaches the fibre housing and is diffused into the WLS fibre. A fraction of the isotropically fluorescent light is captured by the fibre and guided by total internal reflection to the readout system. The same fibre collects the light from all the scintillator plates of the same calorimeter tower. This technique was pioneered by Pretzl and collaborators [4] who proposed to use WLS rods for tower calorimeters. The current technology, first developed by a group from INR-Moscow and IHEP-Protvino [3], allows the use of small diameter fibres instead of rods for reduction in dead space and improvement of uniformity of response. The number of WLS fibres needed for a calorimeter module is determined by the requirement of the maximum light collection efficiency (which in turn determines the uniformity of response of the module as a function of the position), by the cost and practical construction considerations. In particular it is important that the distance between nearby fibres is much less than the effective attenuation length of light into the scintillator.

We have built and tested a prototype of this calorimeter for the CERN experiment WA-96 (NOMAD) [6]. The experiment, to be installed in the CERN ν_μ-beam, aims at the detection of possible $\nu_\mu \leftrightarrow \nu_\tau$ oscillations, by the interaction of the ν_τ with an active target and the detection of the τ^- in the electronic, muonic and hadronic decay channels. The requirements of the experiment on the e.m. calorimeter are: a) good spatial granularity (towers of about 10×10 cm^2 transverse size); b) minimal dead space between towers (the calorimeter transverse size is about $3 \times 3m^2$); c) good energy resolution ($\sigma/E \leq 10\%/\sqrt{E}$); d) low π/e contamination ($\leq$ few 10^{-3}); e) the calorimeter must operate in a magnetic field ($B \approx 0.4$ T). All the above demands are satisfied by a sampling calorimeter with WLS fibre readout. Its large efficiency in collecting the scintillation light greatly reduces the problems of readout in magnetic field. The cost of such a calorimeter, due to the simplicity of construction and the automatisation of machining the individual pieces is comparable to that of calorimeters of more standard design.

We have cross-checked the measured properties of the calorimeter with a Monte Carlo program based on GEANT [5] that simulates the calorimeter's sampling structure and its light collection system.

0168-9002/93/$ 06.00 © 1993 – Elsevier Science Publishers B.V. All rights reserved

2. Description of the calorimeter module

2.1. Geometry and sampling structure

A calorimeter tower is made of a stack of alternating lead and scintillator tiles. Each tile has a square front face of 100×100 mm^2 with 100 holes drilled in it. The holes are arranged in a 10×10 array so that they are uniformly spaced and distributed all over the surface of the plate. The centre of the first hole is 5 mm from the border of the tile and the distance between the centres of two consecutive holes is 10 mm. The pattern of the holes is the same for the plates of the two different materials. The scintillator and lead tiles were provided already cut, drilled and polished by Pol.Hi.Tech [#1].

The firm used a POLIPOP 0181 scintillator with light yield equivalent to NE110, but shorter attenuation length, whose emission spectrum is maximum at 420 nm, well matched with the absorption spectrum of WLS fibres. The holes in the scintillator tiles (1.2 mm diameter) were not polished so as to act as a diffusive surface and improve the light collection efficiency of the fibres. A low weight paper sheet (4 mg/cm^2 density) covered the tiles to diffuse the light. We used 4 mm thick scintillator plates for all the modules we have built.

The lead tiles contained 5% antimony to improve their mechanical properties and the holes were 1.3 mm diameter. The accuracy of the diameter and pattern of the holes is better than 0.05 mm.

The WLS fibres were also provided by Pol.Hi.-Tech. [#2]. The fibres (1 mm diameter), made of polystyrene doped with K27, shift the light in the green and have an attenuation length greater than 1.5 m. We checked, by testing a random sample of fibres, that the attenuation length of the fibres was the same within 10%.

The diameter of the holes in the scintillator and lead plates was optimised to cope with machining tolerances and to make the assembling of each tower easier.

We built calorimeter towers with two different sampling structures: nine modules were built using 1.5 mm thick lead plates [standard modules] and one module with 3 mm thick lead tiles [short module]. In both cases we used 4 mm thick scintillator and the total thickness of the tower was about the same (20 X_0). The stack of a standard (short) tower is made of $75 + 75 (38 + 38)$ layers of alternating lead and scintillator plates for a total length of 412.5(266) mm.

The short module is cheaper and faster to assemble, but has a less favourable sampling fraction with respect to the standard one and is also worse in terms of photon statistics.

2.2. The mechanical assembly

The modules are built by aligning the tiles with steel rods (1.1 mm diameter) inserted in place of a few WLS fibres in the hole pattern. Once all the tiles of a module are piled up, the stack is pre compressed to remove residual air gaps between tiles and wrapped in a 20μm thick aluminium foil. The stack of lead and scintillator tiles is kept as whole block using two 100×412.4 mm^2 stainless steel bands 150μm thick. The bands are on two opposite sides of the tower and are screwed on anticorodal plates located at the ends of the stack (fig. 1).

Each base plate is 6 mm thick and has the same dimensions and holes pattern (1.5 mm diameter) as the lead and scintillator tiles. The base plate, put on the rear face of the tower, is forced away from the stack by three bolts. The bolts are screwed into the base plate and press on a second anticorodal plate put on the stack. Acting on the bolts it is possible to adjust the pressure on the stack. The tiles in the tower are kept together by the friction force. To test the stability and rigidity of the assembly, a tower was put lying horizontally held only by the two extremities for several days. No changes were found in the sagitta, displacement of the tiles and stress acting on the lateral bands after the test period.

When assembling the calorimeter the modules can be arranged such that the two steel bands are never adjacent. In this way dead space between two nearby towers is minimised and we measured the gap between towers to be less than 500μm. (This was mainly due to the fact that each test module was wrapped individually in black tape to make the test beam operation easier. The modules for the NOMAD calorimeter do not need to be individually light hermetic and dead space can be further reduced.).

The WLS fibres were inserted in the calorimeter tower already assembled with the bolts put under pressure. The steel rods used for alignment were removed and replaced with WLS fibres.

Each fibre runs twice along the calorimeter stack. It starts from the rear face, runs for the whole length of the tower in a channel made of aligned holes of the tiles and comes out from the front face of the calorimeter. At this point the fibre is bent and makes an almost circular loop of 25 mm radius entering again in a hole corresponding to a channel on the same row, shifted by five channels from the forth trip hole. After cross-

[#1] Pol.Hi.Tech. s.r.l. S.P. Turanense km 44.400, 67061 Carsoli (AQ), Italy.

[#2] The fibres were of the type POLIFI S050-100, with maximum absorption at 420 nm. The K27 dopant used in the fibres has an emission spectrum peaked at 500 nm.

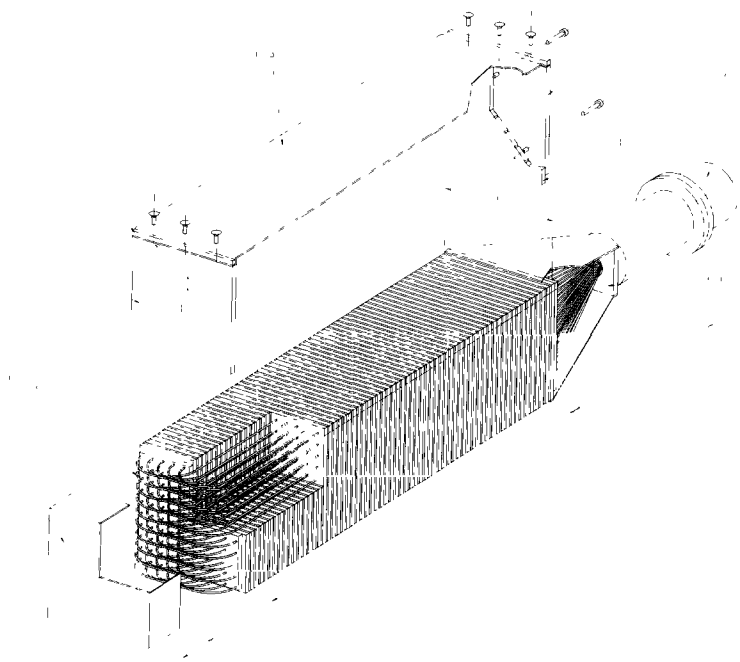

Fig. 1. Exploded view of a calorimeter tower. The support structure of the pile of the lead and scintillator tiles is shown above the calorimeter body (A: end plates, B: 0.15 mm steel band, C: second back plate to squeeze the pile of tiles). The fibres' loop (D) is protected by a cap (E) The fibres are collected at the back of the tower by a pyramidal structure (F) holding the readout device (G).

ing again the whole stack the fibre comes out from the rear face. In fact the fibres were bent before inserting them in the calorimeter. We used a procedure consisting in adiabatic bending in warm silicone oil (at 70°C for eight hours). This process produces permanently bent fibres without damaging the cladding or altering the transmission coefficient of the fibre. We checked that only 5% of light is lost in the loop and therefore the loop acts as an almost ideal mirror.

A light metallic cap protects the fibre's loop from accidental breaking. At the rear face of the tower the fibres are glued together, cut and polished.

Each module is made of the stack of tiles, the front cap to protect fibres loops, and a pyramid frustum at the rear end to collect and hold the bundle of fibres and to hold the readout device. Table 1 summarises the amount of material in the two calorimeter prototypes.

Table 1
Summary of materials used in the calorimeter

Material	Thickness		
	[mm]	$[X_0]$	λ
Front plate	6	0.067	0.016
Lead tile	1.43 (2.9)	0.26 (0.53)	0.0074 (0.015)
Scintillator tile	4	0.01	0.0054
Diffusive paper	2×0.05	≈ 0	≈ 0
Total Standard	418	20.32	0.98
Total Short	266	20.5	0.775

A LED was mounted in the back of each tower, near the bundle of fibres to test the readout system and to make raw calibrations of the calorimeter light output.

The calorimeter was equipped with several readout systems: photomultipliers, silicon photodiodes, avalanche photodiodes and tetrodes. We will report in the following sections the results obtained and discuss the advantages of the different schemes.

3. Experimental conditions

The calorimeter was tested at the T9 beam line of the CERN PS accelerator, with electrons, pions and muons in the energy range from 2 to 8 GeV. The impact point of particles on the calorimeter was measured with an accuracy of 200μm by two drift chambers placed just before the detector. Electrons were discriminated from pions by two Cherenkov counters on the beam line. The pion contamination in the elec-

tron sample was computed to be nearly 1% at 2 GeV and 0.2% at 6 GeV. The beam intensity was typically about 100–200 electrons/burst at 6 GeV, while pions were about ten times more abundant. An almost pure muon beam was obtained by filtering away hadrons and electrons with an absorber of several absorption lengths on the beam line. The muon rate was about 1–5 μ/burst.

The trigger was made by the coincidence of two scintillation counters and a veto counter. The first counter (S1) was located several meters before the calorimeter. A veto counter (V) (a scintillator plate with a hole of 1 cm radius), was located nearly 10 cm before the calorimeter and the second counter (S2), a small scintillator disk of the same radius as the veto hole, was placed immediately after the veto counter.

The calorimeter modules were mounted on a table allowing precise vertical and horizontal movements. Angular scans were also possible.

The CAMAC DAQ chain was made of LeCroy ADCs (models 2249A, 2249W) controlled by an OS9 system[#3]. The OS9 provided data taking and a first on-line analysis of data. Raw data were sent to a SUN workstation and saved on tape for off-line analysis. The workstation also provided graphical facilities for on-line analysis.

4. Results

As mentioned in the introduction the calorimeter is intended to operate in a magnetic field and the design and the performance of a readout system that can operate safely in magnetic field is a problem by itself. We have studied separately the optimal characteristics of the calorimeter using photomultipliers. Individual modules have been tested with readout systems that are able to operate in magnetic field: silicon photodiodes, avalanche photodiodes and tetrodes. Due to lower amplification these devices have to be coupled to low noise preamplifiers with a long shaping time. Consequently the calorimeter performance deteriorates, still matching the experiment's demands.

4.1. Intrinsic properties of the calorimeter

The intrinsic properties of the calorimeter were studied with a 3×3 array (a nonet) of standard modules equipped with EMI-9009 photomultipliers. The optical contact between the fibre bundle and the photomultiplier was ensured by a silicone disk. The modules were pushed to be close to each other by a metallic frame. Dead space between modules was measured to be less than $500\mu m$.

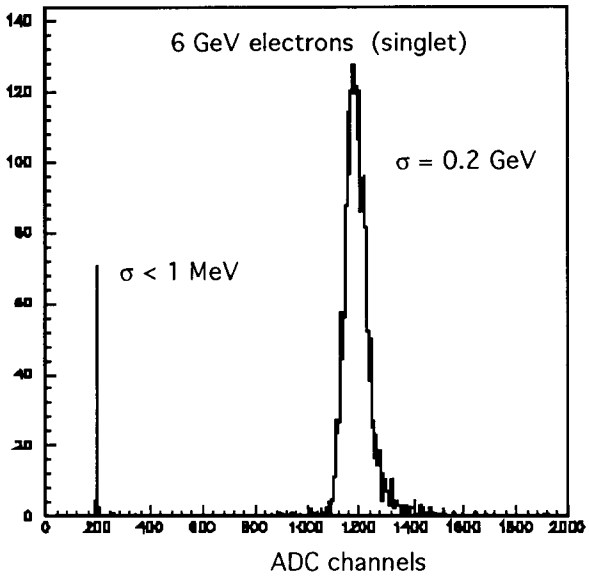

Fig. 2. Charge spectrum of 6 GeV electrons (single module equipped with a photomultiplier).

(i) The linearity of the response was measured with electrons of energies from 2 to 8 GeV. The particles impinged perpendicularly on the central module of the nonet in its centre. A typical charge spectrum of the central nonet module for 6 GeV electrons is shown in fig. 2. The electron peak is well parametrized by a Gaussian with negligible tails. The average charge measured by a single module in ADC channel units is plotted in fig. 3a, versus the beam energy. A linear fit is superimposed to the experimental data. Deviations from linearity are measured by the ratio

$$(Q_{\text{average}} - Q_{\text{fit}})/Q_{\text{average}}$$

and are shown in fig. 3b, as a function of beam energy. Non-linearity effects are less than 1%.

(ii) The ratio of the root mean square (r.m.s. or σ) of the charge collected by a single module to the average charge (σ/E) is shown, as a function of $1/\sqrt{E}$, in fig. 4. Here and in the following we will fit the experimental resolution with the following expression:

$$\sigma/E = \sqrt{(\alpha/\sqrt{E} + \beta)^2 + (\gamma/E)^2}, \qquad (1)$$

where α accounts for sampling fluctuations and photostatistics, β is the "constant" term that includes effects due to leakage, non-uniformity etc. and γ is due to electronic noise.

We obtain $\alpha = 0.0679$ and a constant term $\beta = 0.0093$ and $\gamma \approx 1$ MeV. The energy resolution for electrons sent to the centre of the central module is

[#3] OS9 is made by Creative Electronic Systems S.A. 70, route du Pont-Butin, PO Box 107 CH1213 Petit-Lancy Geneva Switzerland.

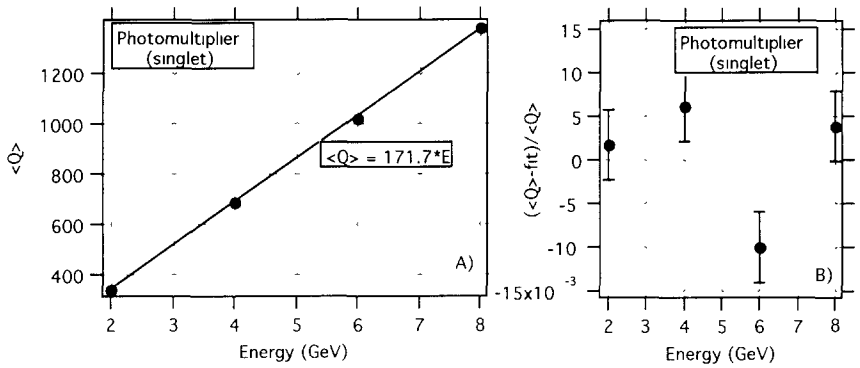

Fig. 3. (a): average charge measured by a single calorimeter module as a function of beam energy. (b): residual of the average charge from the linear fit (b).

improved if we use the charge collected by the whole nonet which accounts for the lateral leakage from the central module. We find $\alpha = 0.0522$, $\beta = 0.013$ and $\gamma \approx 1$ MeV. The lateral leakage at 6 GeV was measured to be about 8% of the response of the central module. The increase of the value of the constant term is compatible with the uncertainty of the relative module to module calibration.

The GEANT Monte Carlo simulation of the calorimeter confirms these results. The energy resolution of a single tower gives $\alpha^{s}_{MC} = 0.067$. A fraction of the energy (about 7.4%, independent of the energy) leaks from the central to the nearby towers. The energy resolution of the nonet gives $\alpha^{n}_{MC} = 0.056$. The dispersion of the transverse leak precisely accounts for the poorer quality of the single tower energy measurement. The effective Molière radius of the calorimeter is found to be $R_M = 3.1$ cm. The longitudinal development of the electromagnetic shower accounts for another source of uncertainty. Fig. 5 shows the average energy deposited in each scintillator tile for electrons of different energies. From these results we compute that, in the energy range from 1 to 10 GeV, about 2.5% of the electron energy escapes from the back of the calorimeter and remains undetected. The distribution of the longitudinal energy leak has a dispersion: $\sigma^{L}_{MC} = 1.011E_e$. This effect is the origin of the "constant term" (β) of the energy resolution.

(iii) The nonet average charge as a function of the beam position in a 2 cm area in its centre is shown in fig. 6. The 1% modulation with a 1 cm pitch is related to the fibre position.

In the boundary between two modules the nonet response drops of 9% from the central module value (fig. 7). Most of this loss (−7%) is confined in a ±2 mm region across the boundary. The energy resolution of the nonet response is also measured as a function of the impact point and, in the worst conditions, at the border of a tower, the term α increases to about 10%.

The calorimeter response can be corrected for this effect if the impact point is measured by an independent detector, as in the case of NOMAD. In this case we have checked that non-uniformity can be reduced to less than 2%. Alternatively we can exploit the granularity of the calorimeter and the finite transverse dimension of the electromagnetic shower to extract from

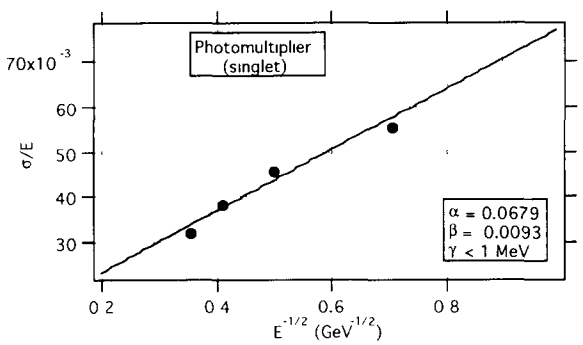

Fig. 4. σ/E as a function of $E^{-1/2}$ (single module).

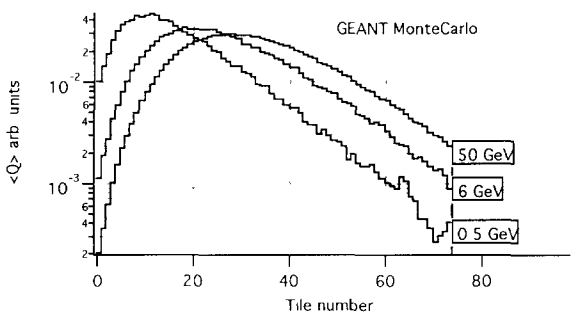

Fig. 5. Average energy deposited in the scintillator tiles for different electron energies.

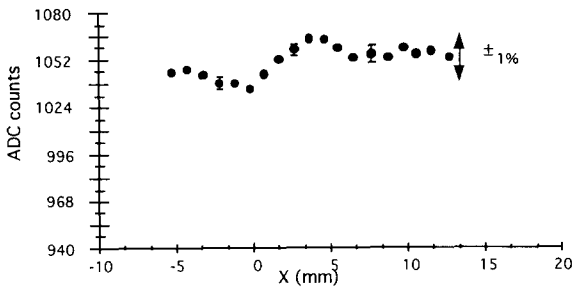

Fig. 6. Nonet charge as a function of beam impact position (centre of the central module).

the distribution of energy in nearby towers the position of the e.m. centroid. The centroid of the electromagnetic shower is defined as the weighted sum of single cell coordinates.

$$\xi_{\text{centroid}} = \sum_i (x_i E_i) / \sum_i E_i .$$

In fig. 8 the shower centroid is plotted as a function of the impact position measured by the beam chambers. The centroid coordinate has a weak dependence on the impact point when the electron hits the central region of the module while there is a sharp dependence in the boundary zone. The GEANT Monte Carlo reproduces these results. The line superimposed to data in fig. 8 is a best fit to 6 GeV Monte Carlo data[#4] The accuracy of the impact position reconstruction is shown as a function of ξ in fig. 9. In the same figure we have plotted the corresponding values for x_{true} and the Monte Carlo predictions. The accuracy in impact

[#4] We have used a function of the type:

$$\xi = \frac{1}{2}\left(k\frac{\sinh(x/\lambda_1)}{\sinh(L/\lambda_1)} + (1-k)\frac{\sinh(x/\lambda_2)}{\sinh(L/\lambda_2)}\right),$$

where k, λ_1 and λ_2 are free parameters, L is the half width of the cell.

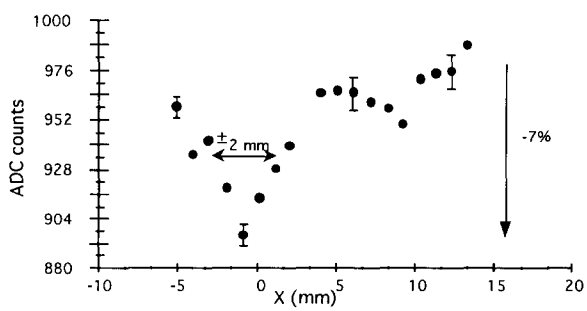

Fig. 7. Nonet charge as a function of beam impact position (boundary of two modules).

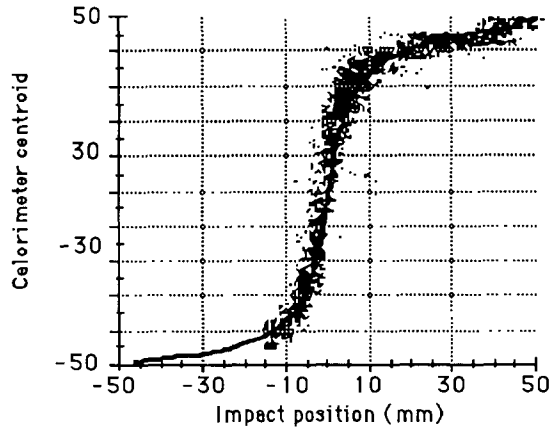

Fig. 8. Shower centroid as a function of beam impact point.

position reconstruction is about 1.3 mm at the boundary of two modules and is adequate to correct for the calorimeter's non-uniformity in this region.

(iv) The calorimeter response as a function of impact angle has been measured at 2 and 6 GeV (fig. 10). (The beam impinged on the central module at its centre). The calorimeter response drops faster, as a function of impact angle at low energies (3% loss at 15° for 6 GeV electrons, compared to 7% loss for 2 GeV electrons). This behaviour is due to the material (stainless steel bands) between modules. Also in this case, the calorimeter response can be corrected for if the impact angle is measured by an independent detector. The nonet resolution is measured to be nearly independent of beam impact angle.

(v) The number of photons collected by the fibre system per GeV of deposited energy was measured with two different methods:

– In the laboratory we measured the number of photons produced in each LED pulse by replacing

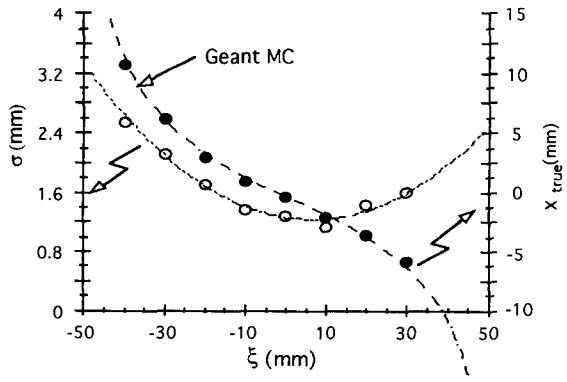

Fig. 9. Accuracy of centroid reconstruction as a function of beam impact point.

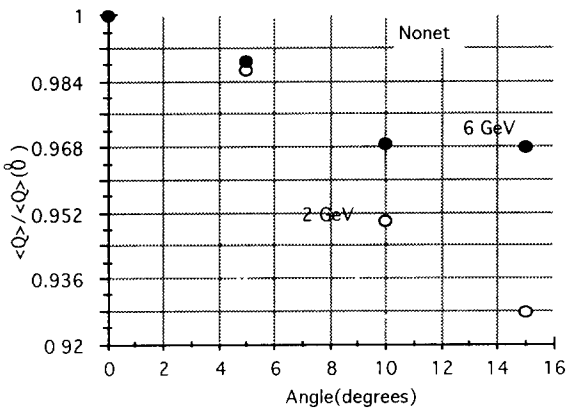

Fig. 10. Calorimeter response as a function of beam impact angle.

the photomultiplier with a calibrated photodiode. By comparing the LED and beam signal at a given energy we could compute that the light yield was greater than 6000 photons/GeV.

– We measured the beam signal at a given energy with and without a light attenuator filter put between the fibre bundle and the photomultiplier. From the two measurements of σ/E we could compute:

$$(\sigma/E)_{\text{nofilter}} = \sqrt{1/N + A^2},$$

$$(\sigma/E)_{\text{filter}} = \sqrt{1/\alpha N + A^2},$$

where we distinguish the contributions to the resolution of photoelectron statistics (N) and of sampling fluctuations (A). α is the attenuation of the filter. By comparing the two measurements we get $N = 1200$ photoelectrons/GeV. Since the quantum efficiency of the photomultiplier in the green is known to be about 15%, we compute a light yield of about 8000 photons/GeV, in reasonable agreement with the previous determination.

(vi) The response of the calorimeter to 6 GeV electrons and pions is shown in fig. 11.

The pion spectrum exhibits a clear minimum ionising peak due to pions that have not interacted in the calorimeter module and leave an average energy of 300 MeV (on the electron energy scale). The pions that interact in the calorimeter begin a hadronic cascade whose broad distribution overlaps in part the electron energy spectrum. A fraction of pions will be mistaken for electrons if their energy deposit in the calorimeter is greater than a given threshold. Setting the threshold such that the efficiency for electrons is 95%, we measure an efficiency for pion detection of 1% at 2 GeV that drops to 0.2% at 6 GeV.

However the electron contamination in the pion sample is also at the level of 0.2%, indicating that, at 6 GeV, the π/e rejection factor is greater than 500.

Measurement of the transverse development of the shower can also improve the π/e rejection factor. We define the transverse radius of the shower as:

$$R = \sqrt{\sum_i E_i R_i^2 / \sum_i E_i}\,.$$

Plots of R versus the nonet energy in ADC counts are shown for electrons and pion at 6 GeV (fig. 12). Electrons populate a region of the plane corresponding to a large energy and a small radius (typically 2 cm). Showering pions fill the region at low energy and radius from 2 to 10 cm. Non interacting pions are constrained in a small region at radius zero and small energy. Due to the electron contamination in the pion beam, a cut on R does not improve on our test beam measurement of the π/e rejection. We estimate that in the case of a pure π beam, a cut on R would improve on the pion rejection by a factor of two.

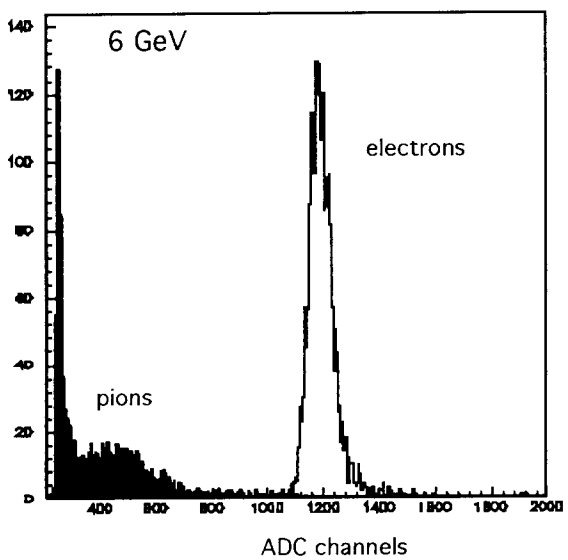

Fig. 11. Calorimeter response to 6 GeV π and electrons.

4.1.1. The short module

The short module has a simplified sampling structure and is made of nearly half of the scintillator and lead tiles used to build a standard module. We expect to have worse results due to the less favourable sampling and the smaller number of photons produced per GeV of deposited energy.

The short calorimeter has been tested with electrons in the energy range 1 to 8 GeV. The calorimeter proved to be linear, with deviations from linearity smaller than 1.3% The energy resolution of this calorimeter is worse than the standard one, mainly be-

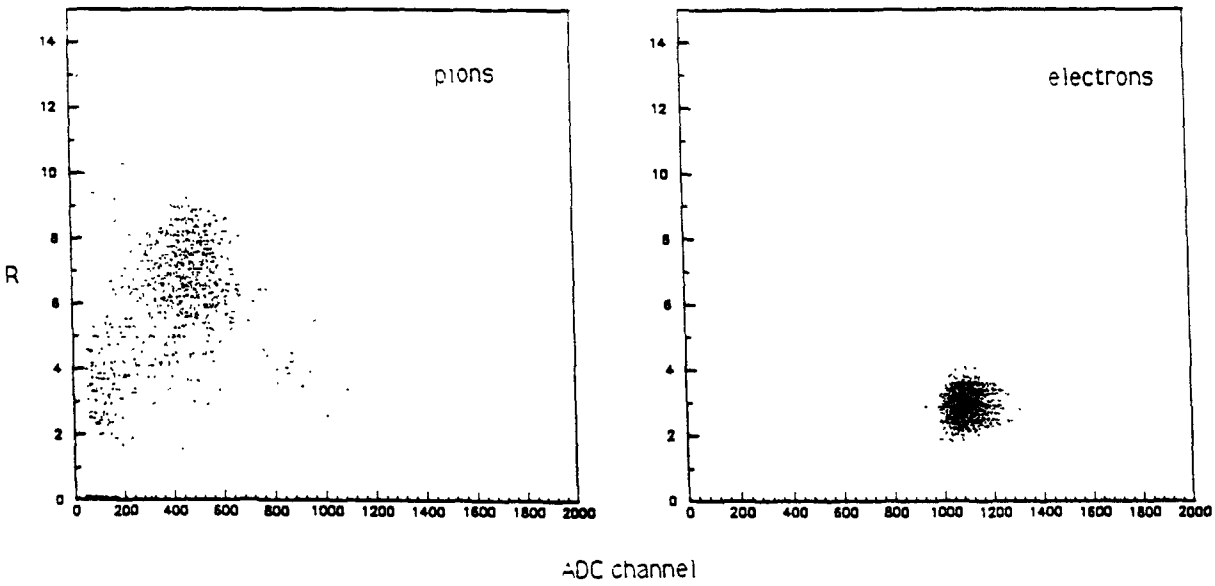

Fig. 12. Transverse radius as a function of nonet energy (6 GeV e and π).

cause of the sampling fraction. Fitting eq. (1) to the data we get $\alpha = 8.6\%$, $\beta = 0.73\%$ and $\gamma \approx 0$:

$$\sigma/E = 8.55\%/\sqrt{E} + 0.73\%.$$

The contribution of the sampling fraction term is larger than in the standard module, as expected, but is still acceptable. We have however to remark that the light yield in the short module is about half of the light yield of the standard one. With readout devices of large amplification and low noise such as photomultipliers the inferior light yield is irrelevant and we measure the small deterioration in energy resolution due to the different sampling fraction. However in case we use magnetic field insensitive readout systems, of lower amplification and larger noise the decrease in the light yield may finally limit the calorimeter performance.

The π/e ratio was also measured. In table 2 we compare the results obtained with the short module with what obtained with the standard one.

Table 2
The π/e ratio Short and Standard module

Energy [GeV]	π/e (Short)	π/e (Standard)
6	0.7%	0.2%
2	1.1%	1.0%

4.2. Silicon photodiode readout

We equipped four modules, including the central module of the nonet, with silicon photo diodes (Hamamatsu S1723-06). Silicon photodiodes are completely insensitive to a magnetic field and have a large quantum efficiency (60% in the green) but also a quite large capacitance (70 pF in the type we used) and unit gain. The photodiodes have been coupled to a low noise charge preamplifier developed by the Lyon L3 group [7] followed by an ORTEC shaping amplifier (model 579) with 200 ns of differentiation time 500 ns of integration time and gain 500 × 0.7. We measured an electronic noise of about 550 electrons which corresponds to about 130 MeV on the electron energy scale.

The response of a single module to 6 GeV electrons is shown in fig. 13. The width of the pedestal is 120 MeV (r.m.s.) in good agreement with the direct measurement of the electronic noise. The ratio σ/E for the single block is 4.45% at 6 GeV a bit worse than the value obtained with the PM (3.9% at the same energy). The energy resolution is plotted as a function of the energy in fig. 14. Fitting the data with eq. (1), we get: $\alpha = 6.9\%$, $\beta = 1.0\%$ and $\gamma = 0.142$ GeV. The value of γ is compatible with the electronic noise measured independently. The values of the α and β parameters differ from the ones measured with photomultipliers but, due to the uncertainty of the fit, the differences are not significant.

Deviations from linearity for a single module are less than 0.7% with the exception of the point at 2

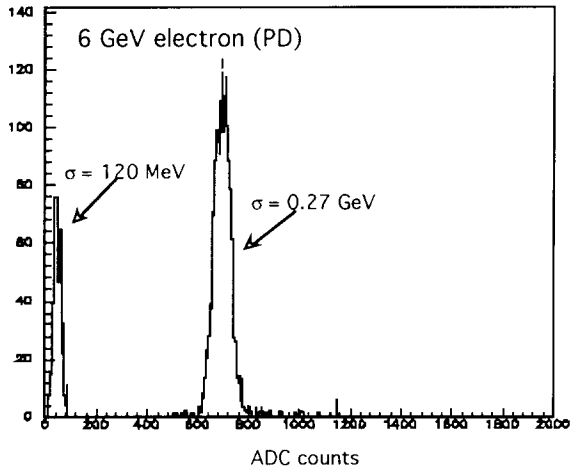

Fig. 13. Response of a single module to 6 GeV electrons (photodiode readout).

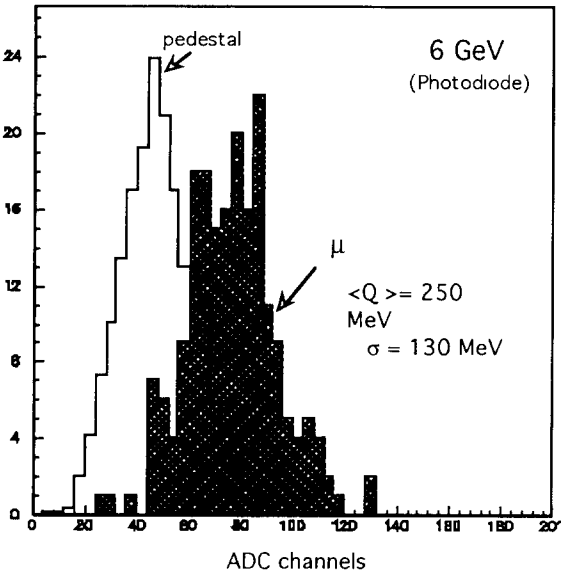

Fig. 15. Pedestal and muon signal (PD readout).

GeV which deviates from linearity of 1.2%.

Fig. 15 shows the pedestal shape and the muon signal distribution. The two peaks are broad because of the electronic noise and are not completely separated. The use of the abundant fluxes of μ in the experimental area was indeed proposed to provide an absolute calibration of the calorimeter. However if the minimum ionising energy loss of muons in the calorimeter is not clearly separated from the ADC pedestal, this calibration method becomes questionable. The present results show that we are probably at the limit for such a method and confirms that the most severe limitations to the use of PD readout is set by the detection of low energy electrons and photons.

The π/e ratio was also measured with the silicon photodiode and gave a result worse than the ratio we could reach with photomultipliers (table 3) because of particle pile-up due to the larger pulse shaping time.

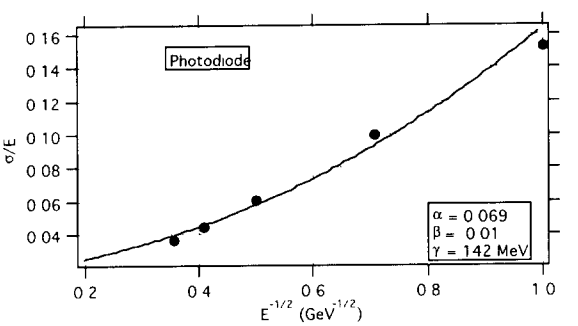

Fig. 14. Energy resolution for a single module (photodiode readout).

4.3. Avalanche photodiodes (APD) readout

Avalanche photodiodes would represent the optimal readout of our calorimeter having, as the photodiodes, good quantum efficiency and total insensitivity to magnetic field and in addition the gain is adjustable up to 5000 by changing the operating voltage. The drawback of this device is a sharp dependence of its gain on the operating voltage and temperature. In addition, as we discovered, the APDs that we have tested are not radiation hard and could be used only for a short time on the beam. We operated the APDs (type 19-13-2/4/6)[#5] at 2400 V corresponding to a gain of about 100–150. The dark current was 0.1μA at the beginning of data taking. The APDs were fed to an ORTEC charge amplifier (model 142) followed by an ORTEC shaping amplifier (model 579) with

[#5] The avalanche photodiodes that we have used are produced by Advanced Photonix, Inc. 1240 Avenida Acaso Camarillo, California 93012, USA.

Table 3
π/e contamination (photo diodes readout)

Energy [GeV]	π/e [%]
2	4.3
4	2.9
6	1.4
8	1.0

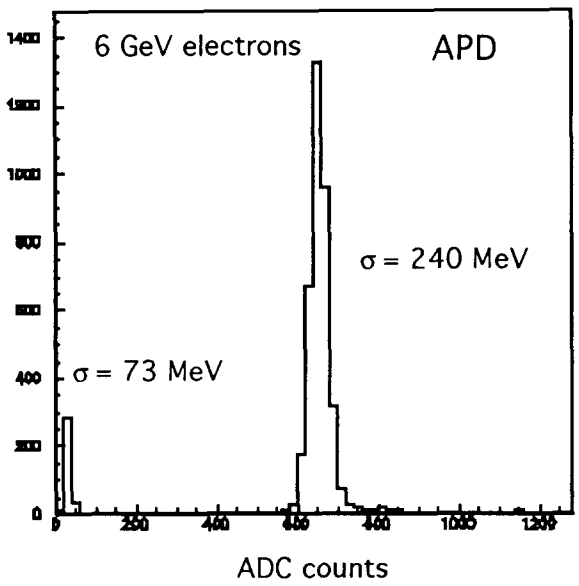

Fig. 16. Response of a module to 6 GeV electrons (APD readout).

T_{diff} = 200 ns, T_{integr} = 200 ns. The noise of the whole electronic chain was equivalent to 23 MeV on the electron energy scale.

The response of a single module to 6 GeV electrons is shown in fig. 16.

The energy resolution is shown in fig. 17 and can be fit to eq. 1, yielding: α = 6.0%, β = 0.65% and γ = 50 MeV.

We tested three APDs in our calorimeter and for all of them, after a short period of exposure to the beam (from 3 to 24 h) the noise suddenly increased by an order of magnitude and the dark current jumped from a fraction of μA to several μA. The huge noise prevented us from taking data any longer. It has been reported to us, after the completion of these tests, that another group [8] has used the same type of APD on a calorimeter. They operated the ADP at low gain (about 20, compared to a gain of 200 in our case), with no problem in stability.

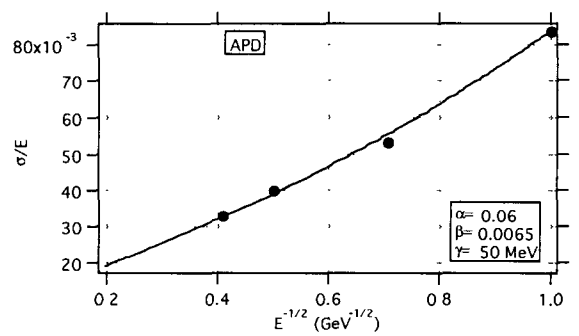

Fig. 17. Energy resolution for a single module (APD readout).

4.4. Tetrode readout

Tetrodes (as well as triodes) are also suited to work in magnetic fields, provided their axis is not perpendicular to $\boldsymbol{B}$ and have indeed been used in calorimeters operated in magnetic fields [9,10]. The gain of a tetrode is low (20–50 for $\boldsymbol{B}$ = 0) but depends mildly on $\boldsymbol{B}$ and on the angle between $\boldsymbol{B}$ and the tetrode axis. At $\boldsymbol{B}$ = 0.4 T and 45° inclination the gain is still 60–70% of the gain at zero field. The central module of the nonet has been equipped with a 1 in. Hamamatsu tetrode type 2149. Tetrodes were fed to a low noise shaping amplifier developed after the design of the DELPHI group [11]. The shaping time was about 1.8μs to keep the electronic noise low.

Fig. 18 shows the calorimeter module response to 6 GeV electrons. The non-Gaussian tails of the distribution originated from particle pile-up. The beam rate in this particular run was large compared to the electronics shaping time. We have checked that the distributions recovered their standard Gaussian shape at low beam rate.

The module response is linear as a function of beam energy; deviations from linearity are smaller than 0.5%. The resolution is similar to what was obtained with the silicon photodiode, but the noise is

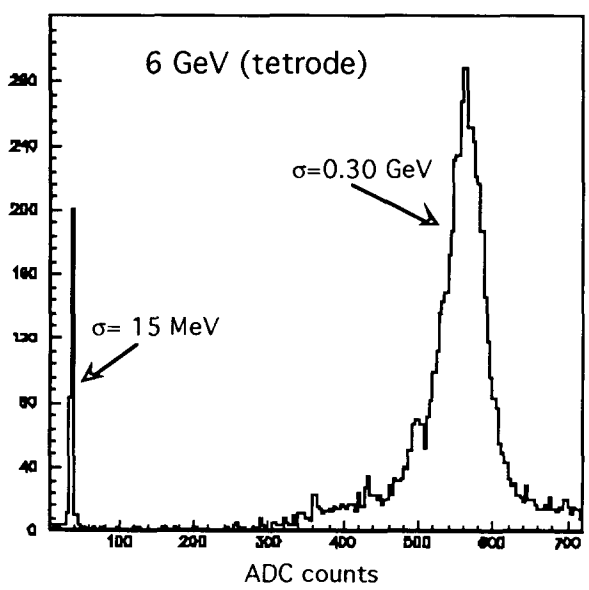

Fig. 18. Calorimeter response to 6 GeV electrons (single module with tetrode readout).

substantially reduced. A fit to the data with eq. (1) yields: α = 9.0%, β = 1.5% and γ = 0.030 GeV. These measurements were performed in non optimised noise conditions. We estimate that, in optimal conditions, the noise term could be pushed down to about 5 MeV.

5. Conclusions

We have built and tested an electromagnetic lead-scintillator sampling calorimeter with light collection by WLS fibres imbedded in the calorimeter module. With this design we could obtain a large efficiency in collecting the scintillation light and virtually no dead space between nearby modules.

The resolution of the calorimeter is limited by sampling fluctuations and is in good agreement with the predictions of a GEANT Monte Carlo simulation.

The calorimeter has a linear response to electron energy and non-linearity are below 1%.

As a function of the impact point, we could observe small non-uniformity of response near the fibre position (less than 1%) and a drop of 7% of the calorimeter response at the border of nearby modules. This effect can be corrected and the response non uniformity is reduced to less than 2%.

The large efficiency in collecting scintillation light ($\sim$ 6000–8000 photons/GeV) allows the use of readout devices less expensive than photomultipliers and capable of working in magnetic fields. We tested photodiodes, avalanche photodiodes and tetrodes. The results for the terms of the resolution formula (1) are summarised in table 4. The calorimeter resolution well matches the requirements of the NOMAD experiment for which the prototype has been built and tested.

Acknowledgements

We gratefully acknowledge the help of our colleagues of the NOMAD collaboration whose cooperation made these tests possible.

We wish to thank Dr. G. Stefanini for his extremely valuable support during the data taking and also for many enlightening discussions to understand the results. In particular tests with the APDs would not have been possible without his essential contribution.

We are very grateful to our technical staff and in particular to A. DiSacco, R. Cosci, M. Favati, M. Iacoponi and E. Pucciarelli.

The Istituto Nazionale di Fisica Nucleare provided the financial support for the construction and the tests of the calorimeter at CERN.

References

[1] S.L. Stone et al., Nucl. Instr. and Meth. 151 (1978) 387.
[2] U. Amaldi, Phys. Scripta 23 (1981) 409.
[3] G.S. Atoyan et al., Preprint INR 736/91 (November 1991).
[4] V. Eckardt et al., Nucl. Instr. and Meth. 155 (1978) 389.
[5] R. Brun et al., DD/EE/81-1 CERN (1987).
[6] P. Astier et al., CERN-SPSLC/91-21, SPSC/P261 11 March 1991;
Addendum CERN-SPSLC/91-48, SPSC/P261 Add 1 21 August 1991;
Addendum CERN-SPSLC/91-53, SPSC/P261 Add 2 25 October 1991.
[7] M. Goyot et al., Nucl. Instr. and Meth. A 263 (1988) 180.
[8] RD1-SPACAL Collaboration, J.M. Gaillard, personal communication.
[9] M. Akrawy et al., Nucl. Instr. and Meth. A 290 (1990) 76.
[10] P. Checchia et al., Nucl. Instr. and Meth. A 248 (1986) 317;
P. Checchia et al., Nucl. Instr. and Meth. A 275 (1989) 49.
[11] G. Barichiello et al., Low noise Amplification Chain of DELPHI End Cap EM Calorimeter, Padova Preprint.

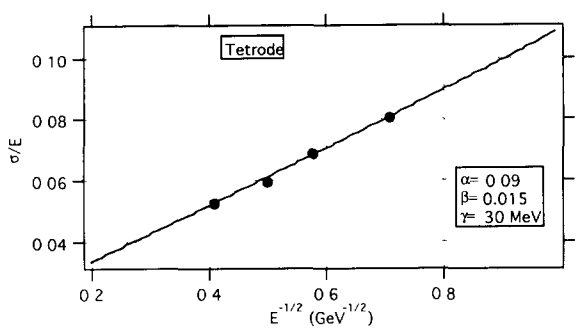

Fig. 19. Single module resolution (tetrode readout).

Table 4
Single tower resolution (σ/E) obtained with the various readout systems

Readout	α [%]	β	γ [MeV]
Photomultiplier	6.63	0.01	0.
Photodiode	6.9	0.01	142.
APD	6.0	0.0065	50.
Tetrodes (see fig. 19)	9.0	0.015	30.